Supporting Information

Hybrid Silicon Nanocrystals for color-neutral and transparent Luminescent Solar Concentrators

Raffaello Mazzaro, Alessandro Gradone, Sara Angeloni, Giacomo Morselli, Pier Giorgio Cozzi, Francesco Romano*, Alberto Vomiero, Paola Ceroni**

1. Materials and methods

All reagents were purchased from Sigma-Aldrich and used without further purification if not stated otherwise. Dry toluene was obtained via distillation over calcium chloride under nitrogen atmosphere. N,N,N',N'-tetramethylethylenediamine was refluxed over fresh KOH and distilled under nitrogen.

For the fabrication of LSCs, methylmethacrylate (MMA, 99%, Aldrich) and lauroylmethacrylate (LMA, 96% Aldrich), purified with basic activated alumina (Sigma-Aldrich), were used as monomers. Lauroyl peroxide (98%, Aldrich) was used as initiators without purification. Ethylene glycol dimethacrylate (EGDM, 98% Aldrich) was used as cross-linker, after purification with basic activated alumina.

Nuclear magnetic resonance (^{1}H-NMR) spectra were measured on an ARX Varian INOVA 400 (400MHz) spectrometer, chemical shifts are reported in ppm and data are reported as follows: chemical shift, multiplicity (s = singlet, d =doublet, t = triplet, q = quartet, br = broad, m = multiplet), coupling constants (Hz). GC-MS analysis were obtained using an Agilent Technologies MSD1100 equipped with EI (70eV) ionization system, single quadrupole analyzer, and HP5 5% Ph-Me Silicon.

2. Synthesis of DPA-functionalized Silicon Nanocrystals

2.1. Preparation of oxide-embedded silicon nanocrystal

Polymeric hydrogen silsesquioxane (HSQ) was prepared from $HSiCl_3$ following reported procedure,[2] dried under vacuum and transferred into a tube furnace. After purging with forming gas (95% N_2, 5% H_2), the tube furnace was heated to 1100°C at a heating rate of 18°C/min and then held at that temperature for an hour. The resulting dark solid was cooled to room temperature, manually reduced into brown powder using mortar and pestle and then transferred to a glass vial half filled with high-purity silica beads and mechanically shaken overnight with a vortex. The resulting homogeneous powder was stored in glass vials until further use.

2.2. Synthesis of hydride-terminated silicon nanocrystals

Hydride-terminated silicon nanocrystals were liberated from the silica matrix through HF etching: 300 mg of oxide-embedded silicon nanocrystals were dispersed in a mixture composed of 3 mL of ethanol, 3 mL of bi-distilled water and 3 mL of a 49% solution of aqueous HF (Note: HF is lethal, handle it with extreme caution). The mixture was stirred for 1h and 30 minutes under ambient light at room temperature. The nanocrystals were extracted with toluene (3x10 mL) and then centrifuged three times in toluene (8000 rpm for 5 minutes). The nanocrystals were then transferred in a dry box.

2.3. Passivation with chlorodimethylvinylsilane or dodecene

The nanocrystals were dispersed in 4 mL of dry toluene and separated in two 8 mL vials. Two milligrams of 4-decyldiazobenzene tetrafluoroborate (about 6 μmol) were added in each one. Afterwards, in a vial, 200 μL of chlorodimethylvinylsilane (1.5 mmol) were introduced to obtain chlorosilane passivated silicon nanocrystals. In the other vial, 330 μL of 1-dodecene (1.5 mmol) were dropped, to passivate the nanocrystals with an alkyl chain. Both mixtures were stirred overnight at RT. The mixture of chlorosilane-passivated SiNCs was then filtered, concentrated at rotary evaporator, transferred again in the dry-box and diluted in 2 mL of dry toluene. The suspension of dodecyl-passivated nanocrystals was precipitated in an anti-solvent (methanol), was centrifuged three times washing with methanol. The precipitate was readily dissolved in 2 mL of toluene.

2.4. Synthesis of (4-(10-phenylanthracen-9-yl)phenyl)methanol

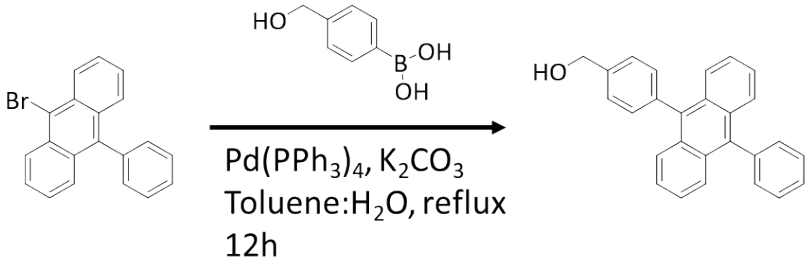

Synthesis of (4-(10-phenylanthracen-9-yl)phenyl)methanol was performed via Suzuki-Miyaura reaction conditions between 9-bromo-10-phenylanthracene and 4-(Hydroxymethyl)phenylboronic acid. To a suspension of degassed toluene (50.0 mL) and K_2CO_3 (12 mL of a 1.6 M solution), under nitrogen atmosphere, 9-bromo-10-phenylanthracene (1.7 g, 5.1 mmol), boronic acid (6.12 mmol, 1.2 equiv.) and a catalytic amount (1.5% m/m) of $Pd(PPh_3)_4$ were added. The resulting mixture was heated at 90°C overnight, then cooled to room temperature, and solvents were removed under reduced pressure at 40°C. The crude was purified via flash chromatography using toluene as eluent and applying a gradient with ethyl acetate to a final ratio of 70:30 (toluene : ethyl acetate). The product was recovered as pale yellow solid after evaporation of solvents, with a yield of 50%. GC-MS m/z: 360.40. ^{1}H-NMR (400 MHz, $CDCl_3$), δ: 7.4-7.6 ppm (17 H, m); 4.90 ppm (1 H, s); 4.71 ppm (2 H, s).

2.5. Synthesis of 9-phenyl-10-(4-((prop-2-yn-1-yloxy)methyl)phenyl)anthracene

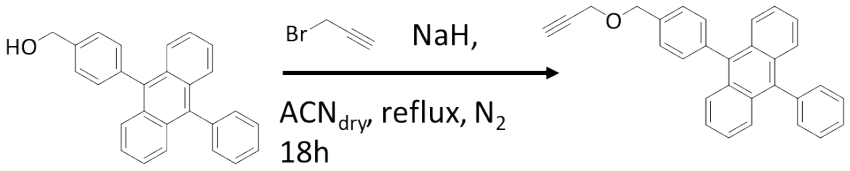

In a two-neck 100 mL round-bottom flask, under nitrogen atmosphere, 75 mL of acetonitrile were introduced to dissolve 1.4 g of (4-(10-phenylanthracen-9-yl)phenyl)methanol (4 mmol). Later, 290 mg of NaH 95% (12 mmol; note: sodium hydride reacts violently with moisture, must be handled under inert atmosphere) were introduced, and the mixture was heated to 78°C. A solution of propargyl bromide (80% in toluene, 1.1 mL, 12 mmol) was added dropwise, and the mixture was stirred at reflux overnight. The reaction was quenched with water (100 mL) and then extracted with DCM (3x100 mL). The organic fraction was collected and dried over $MgSO_4$. A flash chromatography (toluene as eluent phase) was performed to isolate 0.96 g of product, a bright yellow solid (60% yield). GC-MS (EI): m/z 398.51; ^{1}H-NMR (400 MHz, $CDCl_3$), δ: 7-8 ppm (17 H, m); 4.80 ppm (2 H, s); 4.36 ppm (2 H, d, J=4 Hz); 2.55 (1 H, t, J=4 Hz).

2.6. Functionalization of silicon nanocrystals with 9-phenyl-10-(4-((prop-2-yn-1-yloxy)methyl)phenyl)anthracene

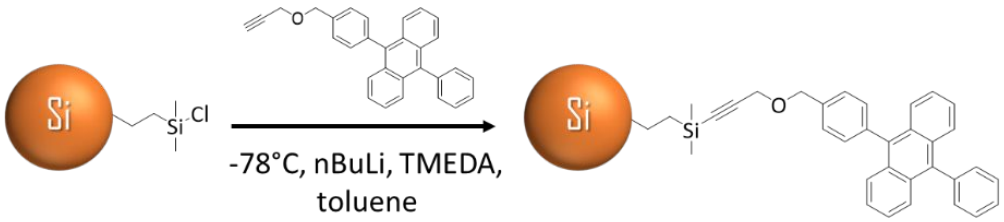

In a two-neck 25 mL round-bottom flask, dried and filled with nitrogen, 120 mg of 9-phenyl-10-(4-((prop-2-yn-1-yloxy)methyl)phenyl)anthracene (0.3 mmol) were introduced. The flask was transferred to a dry-box and 70 µL of N,N,N',N'-tetramethylethylenediamine (TMEDA, 0.45 mmol) and 3 mL of dry toluene were added. The flask was then removed from the dry-box and plugged to a shlenk line filled with N_2. After having cooled the reaction to -78°C with a liquid nitrogen/acetone bath, 120 µL of n-butyllithium (2.5 M in hexanes, 0.3 mmol; note: n-butyllithium reacts violently with moisture, must be handled under inert atmosphere) were added dropwise, while stirring. The acetone bath was removed after 45 minutes, and the mixture was stirred for 15 minutes at room temperature. Again at -78°C, a suspension of silicon nanocrystals in 2 mL of toluene was slowly added to the reaction mixture. One hour later, the acetone bath was removed, and the reaction mixture was stirred for an hour at room temperature. Later, it was heated to 40°C, and stirred for another hour. The reaction was cooled again to -78°C and a second amount of nBuLi (60 µL, 0.15 mmol) was added to complete the capping of the surface. The reaction was allowed to reach room temperature and stirred overnight. The introduction of 7 mL of a 1 M solution of HCl in MeOH made the nanocrystals precipitate. The precipitate was washed 3 times with methanol and separated from the supernatant by centrifuge (8000 rpm, 5 minutes). The nanocrystals were then

dispersed in chloroform, and a size exclusion chromatography over BioBeads™ S-X1 Support (200-400 mesh) in chloroform was performed to isolate a brown limpid suspension.

2.7. ^{1}H-NMR measurements

^{1}H-NMR spectra of the anthracene ligand and the functionalized silicon nanocrystals are reported in Figure S1. The aromatic protons and the ones in α-position with respect to oxygen of diphenylanthracene are present in both spectra, but when the molecule is bonded to the silicon nanocrystal a broadening of the peaks is induced since the movement of the molecules is hindered on the nanocrystal surface. The terminal proton from the alkyne moiety (around 2.5 ppm) reacts in the functionalization and is no longer present in the spectrum of functionalized silicon nanocrystals. ^{1}H-NMR of dodecyl-capped nanocrystals is reported here: ^{1}H-NMR (400 MHz, $CDCl_3$), δ: 1.22 ppm (18 H, m); 0.84 ppm (3 H, s).

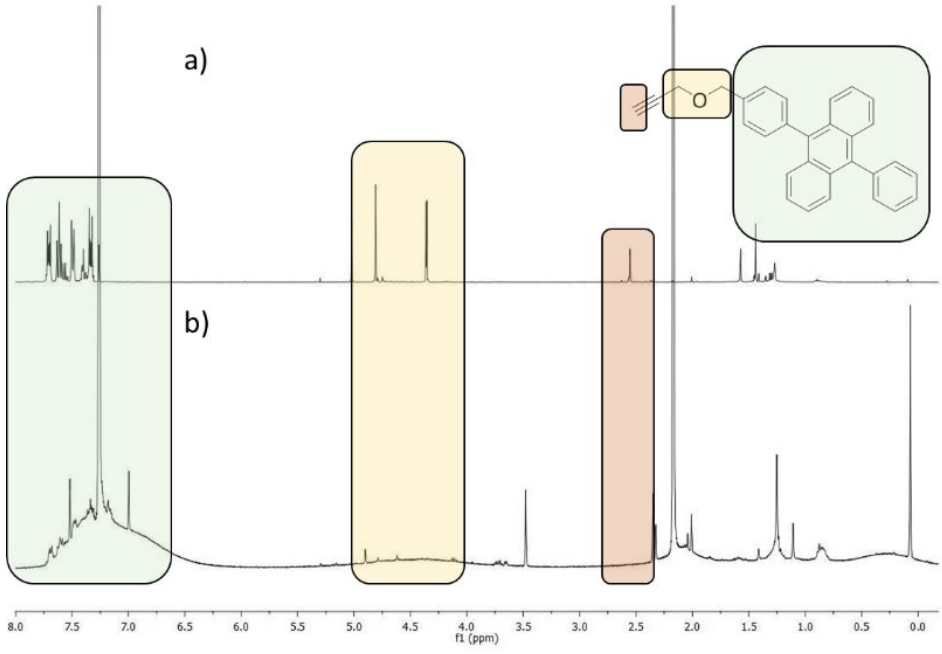

Figure S1. ^{1}H-NMR spectra (400 MHz, $CDCl_3$, RT) a) of 9-phenyl-10-(4-((prop-2-yn-1-yloxy)methyl)phenyl)anthracene, and b) silicon nanocrystals functionalized with 9-phenyl-10-(4-((prop-2-yn-1-yloxy)methyl)phenyl)anthracene.

3. Fabrication of luminescent solar concentrators

The PLMA|PMMA plate was fabricated by bulk co-polymerization, using a "home-made" cell-casting process characterized by two steps. First, the so-called 'syrup' was prepared: LMA monomer was heated in a beaker to 80°C. When the LMA temperature was stable, lauroyl peroxide (0.5% wt/wt with respect to LMA) was added, the pre-polymerization took place and the monomer temperature increased by a few degrees (exothermic process). After 30 minutes, the syrup was quenched in cold water.

In the second step, the MMA monomer, the lauroyl peroxide, the cross-linker (EGDM) and/or the DPA and/or SiNCs were added taking into account this ratio between the components: LMA 35% w/w (prepolimerized); MMA 35 % w/w (monomer); EDGM, 30 % w/w; lauroyl peroxide 0.2% w/w respect to LMA (after the pre- polymerization step).

In order to obtain a homogeneous solution, the reaction mixture was left in ultrasonic bath for 10 min. The reaction mixture was degassed by 3/4 freeze–pump-thaw cycles in order to remove oxygen and nitrogen was purged in every cycle. Finally, the more-viscous liquid was introduced into the casting mould under nitrogen flow, where the polymerization reaction proceeded in an oven at 50°C for an hour and at 80°C for 23h. The casting mould was made by two glass plates sealed with a silicone gasket (to preserve the inert atmosphere) and clamped together.

The main advantage of this approach compared to a photoactivated polymerization is to avoid photodegradation of chromophores like DPA that absorb in the same spectral region of the most commonly used photoinitiators. In addition to that, a method like this requires a very limited amount of radical initiator, which is mostly responsible for photoluminescence quenching while the pre-polymerization step reduces the formation of heterogeneities in the co-polymer.

4. Photophysical measurements in solution

Photophysical measurements were carried out in air-equilibrated distilled toluene at 298 K. UV-visible absorbance spectra were recorded with a Perkin Elmer λ650 spectrophotometer, using quartz

cells with 1.0 cm path length. Emission spectra were obtained with either a Perkin Elmer LS-50 spectrofluorometer, equipped with a Hamamatsu R928 phototube, or an Edinburgh FLS920 spectrofluorometer equipped with a Ge-detector for emission in the NIR spectral region. Correction of the emission spectra for detector sensitivity in the 550-1000 nm spectral region was performed by a calibrated lamp.[3] Emission quantum yields were measured following the method of Demas and Crosby[4] (standard used: $[Ru(bpy)_3]^{2+}$ in air-equilibrated aqueous solution $\Phi = 0.040$[5] and HITCI (1,1′,3,3,3′,3′-hexamethyl-indotricarbocyanine iodide) in EtOH $\Phi = 0.30$).[6] Emission intensity decay measurements in the range 10 μs to 1 s were performed on a homemade time-resolved phosphorimeter. The estimated experimental errors are: 2 nm on the absorption and emission band maximum, 5% on the molar absorption coefficient and luminescence lifetime, and 10% on the luminescence quantum yield.

The size of the nanocrystals was determined by comparing the energy of the PL band maximum with the size-band gap correlation curve developed in ref.[1] and reported in figure S2.

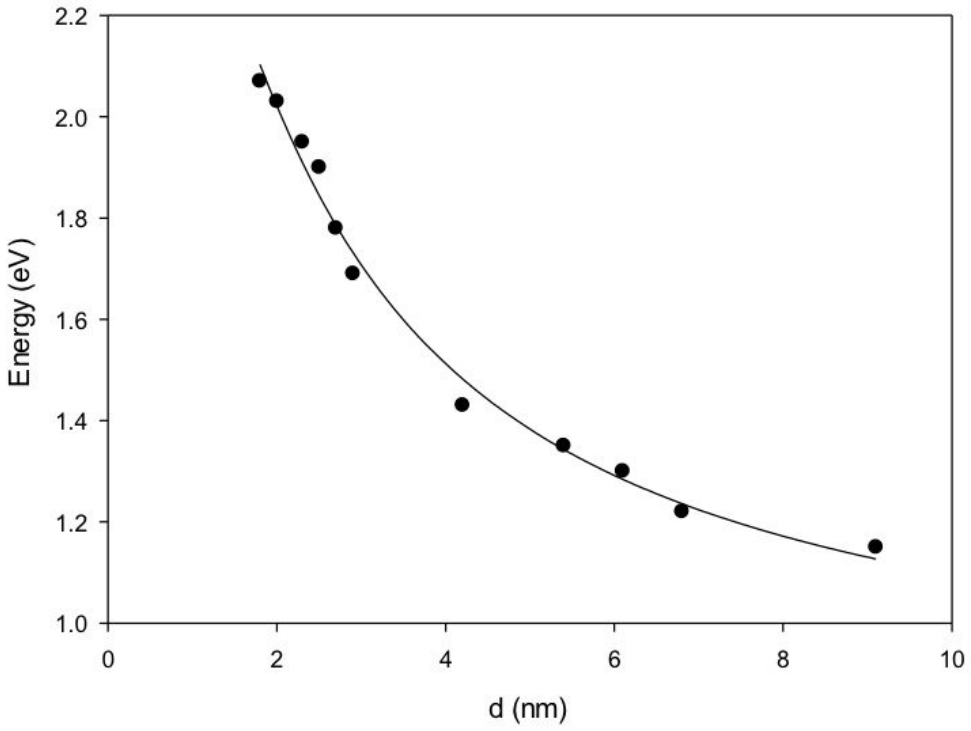

Figure S2. PL peak energy vs. core diameter for alkyl passivated colloidal SiNCs.

4.1. DPA PL quenching efficiency (η_q) in Si-DPA.

The quenching efficiency of the chromophores can be estimated using the equation:

$$\eta_q = \frac{\int_{\lambda = 550nm}^{\lambda = 400nm} I_{Si-DPA}}{\int_{\lambda = 550nm}^{\lambda = 400nm} I_{Si+DPA}} \qquad \text{(S1)}$$

where $I_{DPA-SiNCs}$ is the PL of the covalent sample and $I_{DPA+SiNCs}$ is the PL of the non-covalent DPA + SiNCs mixture. The control sample (**Si+DPA**) is constituted by a physical mixture of **Si** and **DPA** with the same concentration in order to perfectly match the absorption profile of the **Si-DPA** sample (Figure 2).

The two PL spectra, used to estimate the quenching efficiency by equation S1, are acquired exciting at the same wavelength, in which the two solution have the same absorbance.

The quenching efficiency of DPA fluorescence can be estimated also by the decrease of the lifetime of the fluorescent excited state of DPA in **Si-DPA** (τ = 0.8 ns)[1] compared to that of the **DPA** chromophore (τ = 5.4 ns). From these value a quenching efficiency [η_q = 1- (τ/τ^0)] of 85% is estimated, in very good agreement with the result from the steady-state measurements.

4.2. Excitation spectra

The close match of the excitation spectrum performed at the SiNC emission (λem=750 nm) and the absorption spectrum of Si-DPA (**Figure S3**) reveal the presence of a very efficient energy transfer.

[1] In the **Si-DPA** sample we also observe a lifetime of 4.8 ns related to a small amount of free DPA.

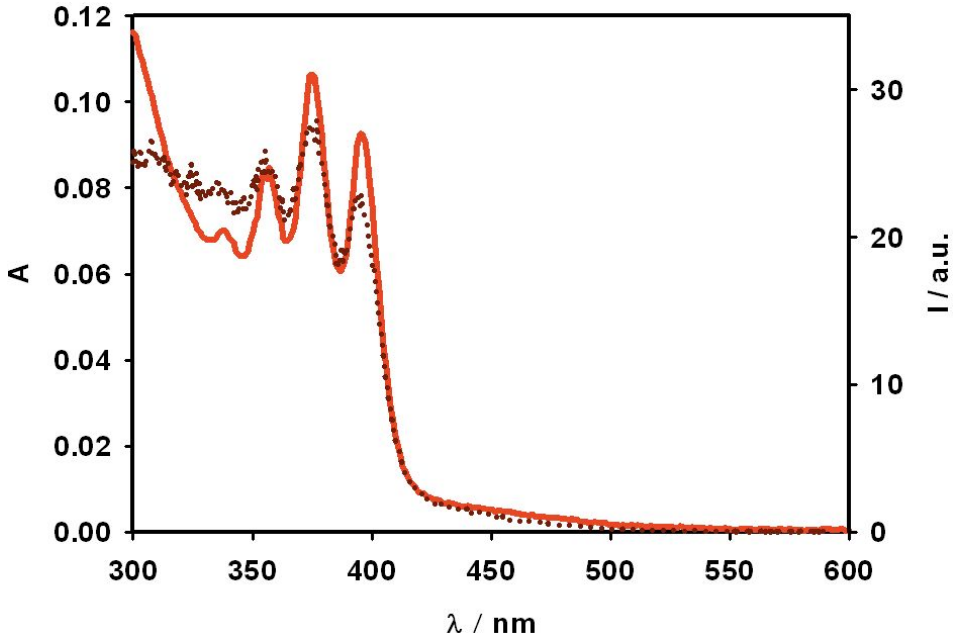

Figure S3. Absorption (red continuous line) and excitation (λ_{em}=750 nm, dark red dotted line) spectra of Si-DPA in air-equilibrated toluene.

4.3. Silicon Nanocrystals Sensitization Efficiency (η_s).

To estimate the energy transfer efficiency, we registered PL spectra of two **Si-DPA** samples displaying the same absorbance at the following excitation wavelengths:

- 375 nm, where most of the light (80%) is absorbed by **DPA**;
- 430 nm, where only the silicon core is absorbing light.

By keeping the experimental conditions constant and correcting for the incident photon flux using an air-equilibrated aqueous solution of $[Ru(bpy)_3]^{2+}$ at the two different wavelengths, the sensitization efficiency can be evaluated as follows:

$$\eta_s = \frac{\int_{\lambda=1000nm}^{\lambda=550\,nm} I_{Si-DPA} - \int_{\lambda=1000nm}^{\lambda=550nm} I_{0\%}}{\int_{\lambda=1000nm}^{\lambda=550\,nm} I_{100\%} - \int_{\lambda=1000nm}^{\lambda=550nm} I_{0\%}} \qquad \text{(S2)}$$

where I_{Si-DPA} is the PL spectrum of the sample **Si-DPA** upon excitation at 375 nm, $I_{100\%}$ is the PL spectrum of the sample **Si-DPA** upon excitation at 430 nm and $I_{0\%}$ represents the amount of light emitted by the silicon core upon direct excitation of the silicon core at 375 nm and is equal to 20% I_{Si-DPA}.

The resulting estimated energy transfer efficiency is 70% in **Si-DPA**.

5. Photophysical measurements on LSCs

UV-Vis transmittance spectra of the prepared LSCs were collected on an Agilent Cary 5000 UV-Vis-NIR spectrophotometer equipped with solid state holder. Color Rendering Index (CRI) and Colour Coordinates were calculated by multiplying the transmittance spectrum to the incident AM 1.5G spectrum, in order to simulate the spectrum of the light transmitted through the LSC:

$$T = \frac{I_T}{I_0} \quad \rightarrow \quad I_T = I_0 \times T \qquad \text{(S3)}$$

The resulting spectra were processed with CIE 13.3 CRI (1994) software© (Péter Sylvester, University of Veszprém) and the obtained coordinates plotted in the CIE 1931 color space chromaticity diagram.

The fraction of photons absorbed in the in the visible region of the solar spectrum ($\lambda_{abs} =$ 400-700) was calculated as follows:

$$\eta_{abs}^{400-700nm} = \frac{\int_{\lambda=400\,nm}^{\lambda=700\,nm} I_0 - I_T}{\int_{\lambda=400\,nm}^{\lambda=700\,nm} I_0} \qquad \text{(S4)}$$

PL spectra were registered with the same equipment described for the solution-phase characterization, but sample holder and excitation source were adapted depending on the specific measurement.

PLQY of the LSCs was calculated with the integrating sphere described by De Mello et al.[2]. A reference polymer slab with the same composition was used as blank sample.

The optical efficiency of the LSC was measured adapting a method previously described by Coropceanu et al.[3] based on the integrating sphere determination. Black tape was used to cover the edges of the LSC and the PLQY was measured in this condition and compared with the one measured on the same LSC with free edges.

5.1. PL lifetime

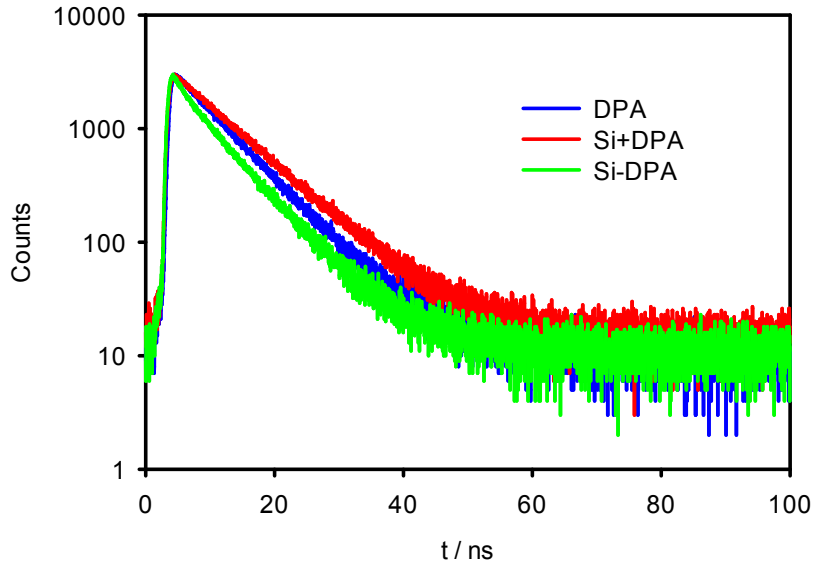

Figure S4. Time-resolved PL intensity of DPA in the prepared LSCs (λexc=375 nm, λem=410 nm) obtained in 45^0 configuration.

5.2. Inner Filter Correction

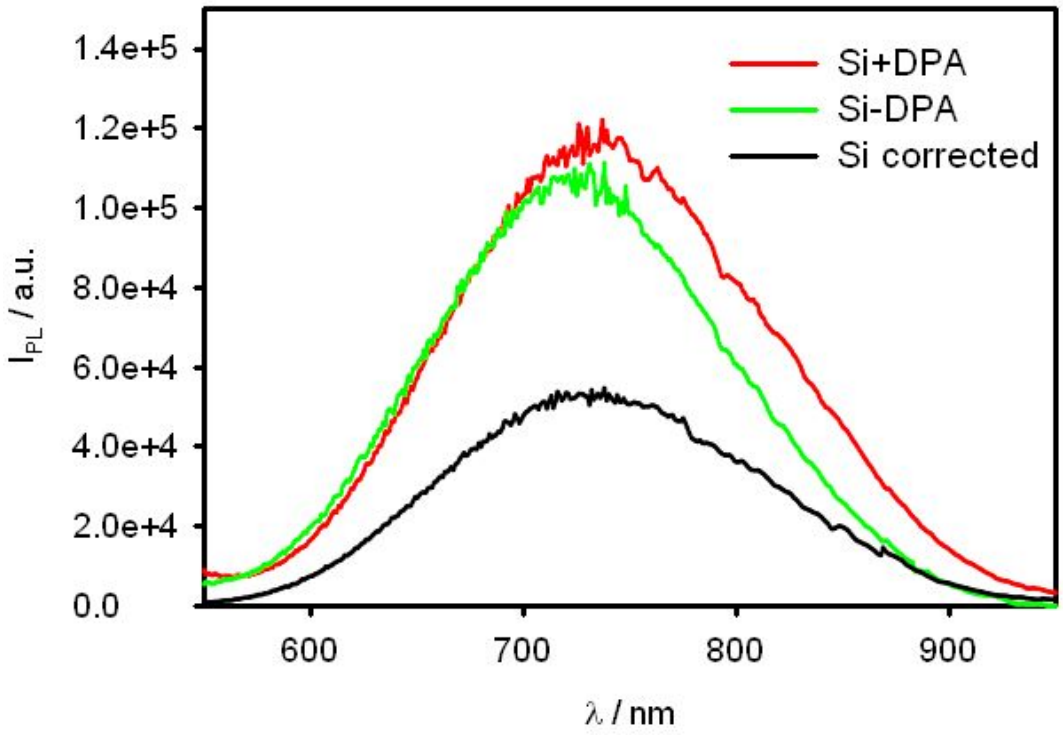

Figure S5. PL spectra of **Si+DPA** (red line) and **Si-DPA** (green line) measured inside an integrating sphere by excitation of the larger surface of LSCs at λ_{exc}=375 nm. **Si** sample PL (black line) is also reported for comparison, after applying the inner filter correction, as described in the main text.

In order to take into account of the inner filter effect[4] and to compare the PL spectra of the **Si-DPA** and **Si+DPA** samples with the one with pristine SiNCs, **Si**, the following correction has to be applied to the latter:

$$I_{1,\ inner\ filter} = I_{1,no\ inner\ filter} \frac{A_1}{A_{tot}} \left(1 - 10^{-(A_{tot})}\right) \qquad \text{(S5)}$$

Where $I_{1,\ inner\ filter}$ is the Intensity measured in the sample with an absorbance equal to A_{tot}, $I_{1,no\ inner\ filter}$ is the calculated value in absence of inner filter effect and A_1 is the absorbance of the investigated specie (SINCs) in the reference mixture (either **Si-DPA** or **Si+DPA**) having overall absorption A_{tot}. **Figure S5** reports the calculated **Si** spectrum following this approach, in comparison with pristine **Si+DPA** and **Si-DPA** samples, both exhibiting higher PL intensity with respect to corrected **Si**.

5.3. PL as a function of optical path

Distance-dependent PL measurements were performed by placing one sample edge perpendicular to the emission monochromator and replacing the fluorimeter excitation source with a monochromatic large area LED or a small spot laser, depending on the measurement. Small spot excitation with a λ=405 nm laser was employed for the band shape determination to maximize the spatial resolution (**Figure S7**; step 5 mm). The laser was mounted on a homemade movable stage perpendicular to the LSC main axis, as displayed in **Figure S6a**, in order to maintain fixed emission position (LSC edge) but tunable excitation source position. For the intensity comparation (**Figure 5**), a fixed, large area, uncoherent source (LED, 375 nm) was employed to fully illuminate the LSC. As for the single point illumination, the LSC position was maintained fixed through the measurement, while the top of the LSC was covered with a black card in order to mask the LSC and allow for a specific area of the LSC to be irradiated. By moving the mask towards the collection edge, the irradiation area was decreased as a function of the distance, as displayed in **Figure S6b**. The observed spectrum was then integrated over the wavelength range of interest (400-550 nm for DPA, 550-1000 nm for

SiNCs) and divided by the area of illumination. The values were finally normalized on the lowest area spectrum integral (1 cm side length) to compare the intensity trend.

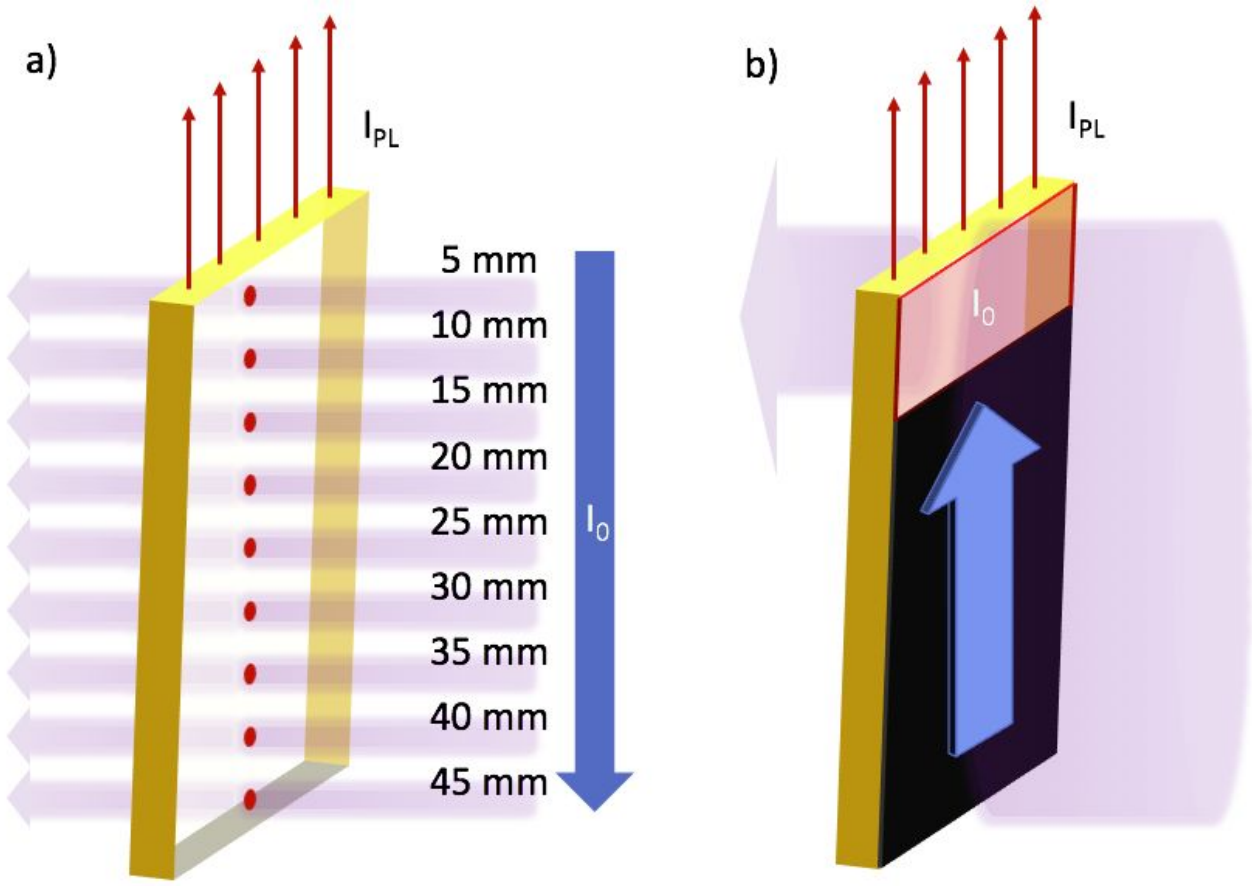

Figure S6. Schematic representation of the distance-dependent PL measurement employed for the determination of the performance of the LSCs with increasing PL optical path. Left, small spot excitation with tunable position; right, large area excitation with movable mask.

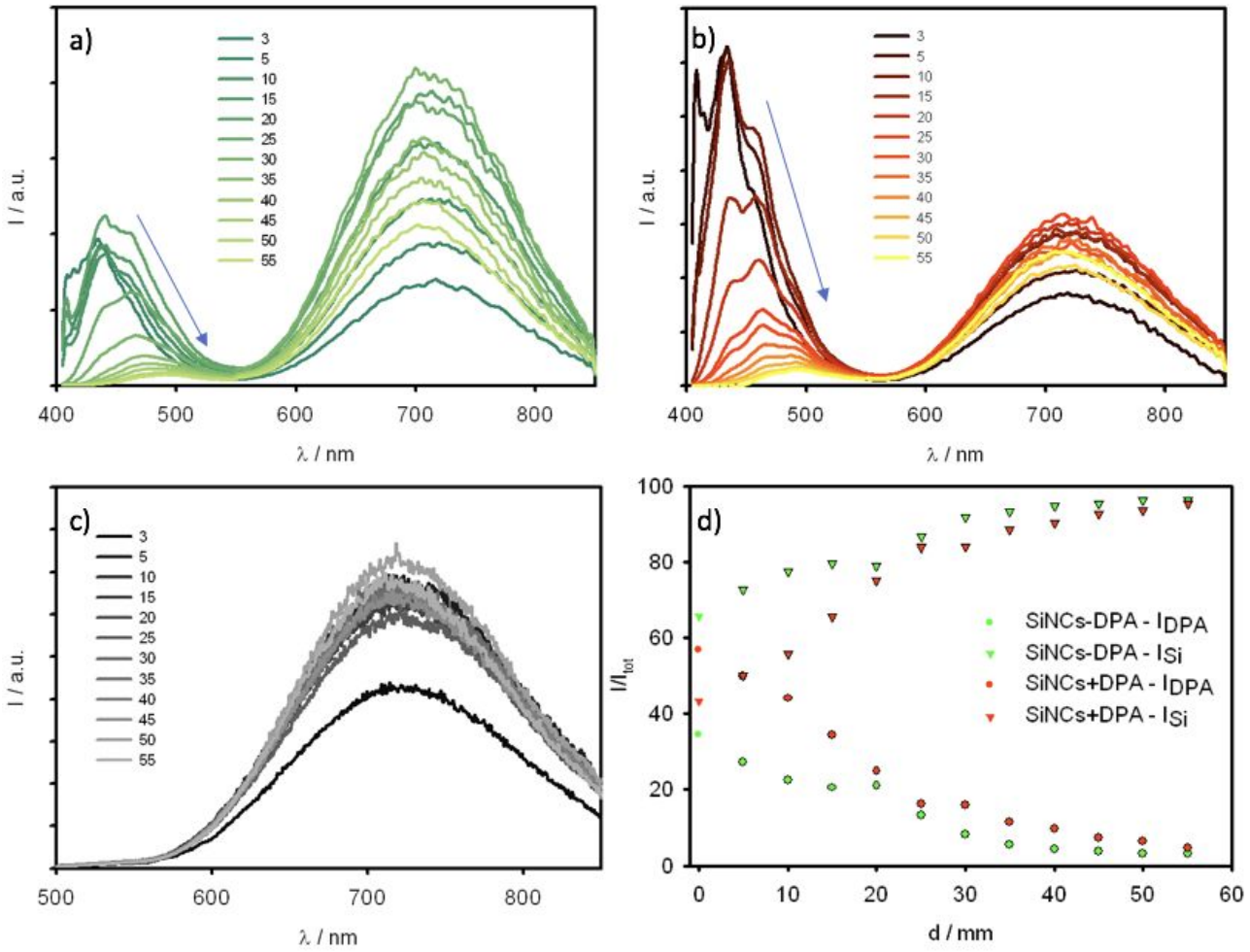

Figure S7. PL spectra of a) **Si-DPA**, b) **Si+DPA** and c) **Si** samples as a function of the distance between the excitation spot on the top of the polymer slab, and the emission area, located on one of the edges of the slab. The distance value is reported in the inset (mm). d) Integrated PL intensity values for SiNCs emission contribution (triangles, λ_{em} = 550-900 nm) and DPA´s emission contribution (circles, λ_{em} = 400-550 nm) obtained from spectra reported in figure 6a (green, **Si-DPA**) and 6b (red, **Si+DPA**). X-axis reports distance between the excitation spot on the top of the polymer slab, and the emission area, located on one of the edges of the slab.

6. Photostability

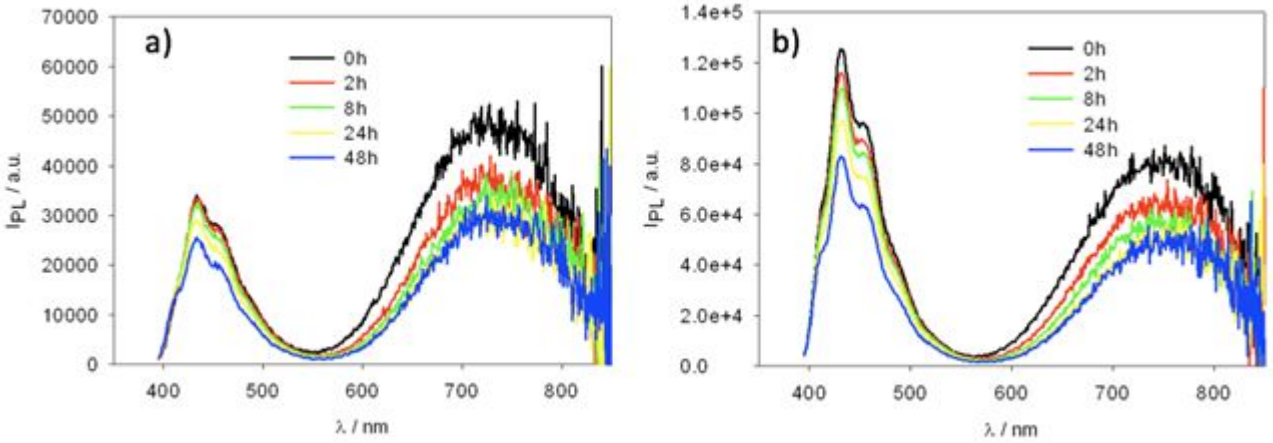

Figure S8. PL spectra of a) **Si-DPA**, b) **Si+DPA** under continuous AM 1.5G irradiation, to assess photostability.

7. Photovoltaic characteristics determination

For the photovoltaic characterization of the LSC devices, a a-Si PV cell was masked, exposing an area of 1.08 cm^2 in order to fully cover the LSC short edge in all samples. The cell was fixed to the side of a homemade black cell and connected to a source picoammeter (Keithley 2401) equipped with a solar simulator. The solar simulator consists in a Xe lamp with an AM 1.5 - Global filter, which can generate vis-UV light with the power intensity of 1 Sun (100 mW cm^{-2}). The light intensity of the solar simulator was controlled through a calibrated silicon solar cell.

The optical contact between the cell and the LSC was optimized by adding a clear tape layer between them, in order to reduce the roughness of the slab and increase the quality of the optical interface. Photovoltaic characteristics in direct illumination configuration of the a-Si cell was performed, obtaining PCE equal to 18.1%, J_{SC} = 44.1 mA and V_{OC} = 592 mV. The G-factor was calculated as follows, by using the size of each LSC reported in table S1:

$$G = \frac{A_{top}}{2A_{edge,\,long} + 2A_{edge,short}} \qquad \text{(S6)}$$

Where $A_{top} = Lxl$, $A_{edge,\,long} = Lxt$ and $A_{edge,short} = lxt$.

	G	**L**	**l**	**t**	$\mathbf{q_{re\text{-}shaping}}$	$\eta_{opt,q}$
Blank	2.86	6.40	2.35	0.30	-	

DPA	2.69	6.10	2.20	0.30	0.75	4.81
Si	2.64	5.70	2.20	0.30	1.07	3.30
Si+DPA	2.56	5.40	2.05	0.29	0.85	3.34
Si-DPA	2.98	5.60	2.15	0.26	0.93	4.98

Table S1. G factor and lateral size of the prepared LSCs, expressed in cm. Re-shaping factor ($\mathbf{q_{re\text{-}shaping}}$), defined as the ratio between the c-Si PV cell EQE over the emission spectrum of the luminophore $\langle Q_{PL} \rangle$ and the EQE over the full solar spectrum $\langle Q_s \rangle$. Optical efficiency corrected for the re-shaping factor ($\eta_{opt,q}$).

The J_{SC} values were normalized for the area mismatch between LSC/PV cell contact area and the exposed area of the cell employed for the direct illumination configuration (i.e. 1.08 cm^2).

The $\eta_{opt,q}$ values were calculated as follows[5]:

$$\eta_{opt,q} = \eta_{opt} \,/\, q_{re-shaping} \qquad \text{(S7)}$$

Bibliography

(1) Yu, Y.; Fan, G.; Fermi, A.; Mazzaro, R.; Morandi, V.; Ceroni, P.; Smilgies, D.-M. .; Korgel, B. A. Size-Dependent Photoluminescence Efficiency of Silicon Nanocrystal Quantum Dots. *J. Phys. Chem. C* **2017**, *121*, 23240–23248. https://doi.org/10.1021/acs.jpcc.7b08054.

(2) de Mello, J. C.; Wittmann, H. F.; Friend, R. H. An Improved Experimental Determination of External Photoluminescence Quantum Efficiency. *Adv. Mater.* **1997**, *9*, 230–232. https://doi.org/10.1002/adma.19970090308.

(3) Coropceanu, I.; Bawendi, M. G. Core/Shell Quantum Dot Based Luminescent Solar Concentrators with Reduced Reabsorption and Enhanced Efficiency. *Nano Lett.* **2014**, *14*, 4097–4101. https://doi.org/10.1021/nl501627e.

(4) Panigrahi, S. K.; Mishra, A. K. Study on the Dependence of Fluorescence Intensity on Optical Density of Solutions: The Use of Fluorescence Observation Field for Inner Filter Effect Corrections. *Photochem. Photobiol. Sci.* **2019**, *18*, 583–591. https://doi.org/10.1039/C8PP00498F.

(5) Li, H.; Wu, K.; Lim, J.; Song, H.-J.; Klimov, V. I. Doctor-Blade Deposition of Quantum Dots onto Standard Window Glass for Low-Loss Large-Area Luminescent Solar Concentrators. *Nat. Energy* **2016**, *1*, 16157. https://doi.org/10.1038/nenergy.2016.157.